Pure appl. geophys. 158 (2001) 1531–1545
0033–4553/01/081531–15 $ 1.50 + 0.20/0

Pure and Applied Geophysics

Automated Detection, Extraction, and Measurement of Regional Surface Waves

A. L. LEVSHIN[1] and M. H. RITZWOLLER[1]

Abstract — Our goal is to develop and test an effective method to detect, identify, extract, and quantify surface wave signals for weak events observed at regional stations. We describe an automated surface wave detector and extractor designed to work on weak surface wave signals across Eurasia at intermediate periods (8 s–40 s). The method is based on phase-matched filters defined by the Rayleigh wave group travel-time predictions from the broadband group velocity maps presented by RITZWOLLER and LEVSHIN (1998) and RITZWOLLER *et al.* (1998) and proceeds in three steps: Signal compression, signal extraction or cleaning, and measurement. First, the dispersed surface wave signals are compressed in time by applying an anti-dispersion or phase-matched filter defined from the group velocity maps. We refer to this as the 'compressed signal.' Second, the surface wave is then extracted by filtering 'noise' temporally isolated from the time-compressed signal. This filtered signal is then redispersed by applying the inverse of the phase-matched filter. Finally, we adaptively estimate spectral amplitude as well as group and phase velocity on the filtered signal. The method is naturally used as a detector by allowing origin time to slide along the time axis. We describe preliminary results of the application of this method to a set of nuclear explosions and earthquakes that occurred on or near the Chinese Lop Nor test site from 1992 through 1996 and one explosion on the Indian Rajasthan test site that occurred in May of 1998.

Key words: Surface waves, Rayleigh waves, matched filters, group velocity, nuclear monitoring, $M_s : m_b$ discriminant.

1. Introduction

The $M_s : m_b$ discriminant and its regional variants are the most reliable transportable means of discriminating earthquakes from explosions. To measure surface wave amplitudes accurately in order to estimate M_s is very challenging for small events in which surface waves may not be readily identifiable in raw seismograms. To provide these amplitude measurements, it is crucial to be able to reliably detect small amplitude surface wave-packets and extract all and only the desired wave-packets reliably so that spectral amplitude measurements can be obtained.

[1] Department of Physics, University of Colorado at Boulder, Boulder, CO, 80309-0390, USA.
E-mail: levshin@ciei.colorado.edu

We describe a surface wave detector and extractor designed to work on weak surface wave signals across Eurasia at intermediate periods (8 s–40 s). It is founded on a long history of surface wave frequency-time analysis (e.g., DZIEWONSKI *et al.*, 1969; LEVSHIN *et al.*, 1972, 1989, 1992; CARA, 1973; RUSSELL *et al.*, 1988). However, successful detection and wave-packet extraction are both dependent on the ability to make accurate predictions of surface wave arrival times at intermediate periods. Our method is based on the Rayleigh wave group travel-time predictions from the recent broadband group velocity maps of RITZWOLLER and LEVSHIN (1998) and RITZWOLLER *et al.* (1998) and proceeds in three steps: Signal compression, signal extraction or cleaning, and measurement.

First, the dispersed surface wave signals are compressed in time by applying an anti-dispersion or phase-matched filter defined from our group velocity maps. We refer to this as the 'compressed signal.' Second, the surface wave is then extracted by filtering 'noise' temporally isolated from the time-compressed signal. This filtered signal is then redispersed by applying the inverse of the phase-matched filter. We refer to this wave-form as the 'filtered' or 'cleaned signal.' Finally, we adaptably estimate spectral amplitude as well as group and phase velocity on the filtered signal. After amplitudes are measured, M_s is estimated using an empirical relation such as that recently presented by REZAPOUR and PEARCE (1998).

The general methodology of matched filtering was developed previously by a number of other researchers (e.g., HERRIN and GOFORTH, 1977; STEVENS, 1986; RUSSELL *et al.*, 1988; STEVENS and MCLAUGHLIN, 1997). We introduce three innovations here: (1) the use of recent group velocity maps to define the matched-filters, (2) automation of the procedure, and (3) the use of the method as a detector.

We describe preliminary results of the application of this method to a set of nuclear explosions and earthquakes that occurred on or near the Chinese Lop Nor test site from 1992 through 1996 and one explosion on the Indian Rajasthan test site that occurred on May 11, 1998.

2. Group Velocity Maps and Correction Surfaces

Elsewhere we have described the construction of intermediate period group velocity maps across Eurasia (e.g., RITZWOLLER and LEVSHIN, 1998; RITZWOLLER *et al.*, 1998), the Arctic (LEVSHIN *et al.*, 2001), South America (e.g., VDOVIN *et al.*, 1999), and Antarctica (e.g., VDOVIN, 1999). The method of tomography and the construction of group velocity correction surfaces is described by BARMIN *et al.* (2001) in this volume. In this paper we will use the somewhat dated group velocity maps presented by RITZWOLLER *et al.* (1998).

Figure 1 displays group velocity correction surfaces computed from the 20 s group velocity map of RITZWOLLER *et al.* (1998) for four stations: AAK (Ala-Archa,

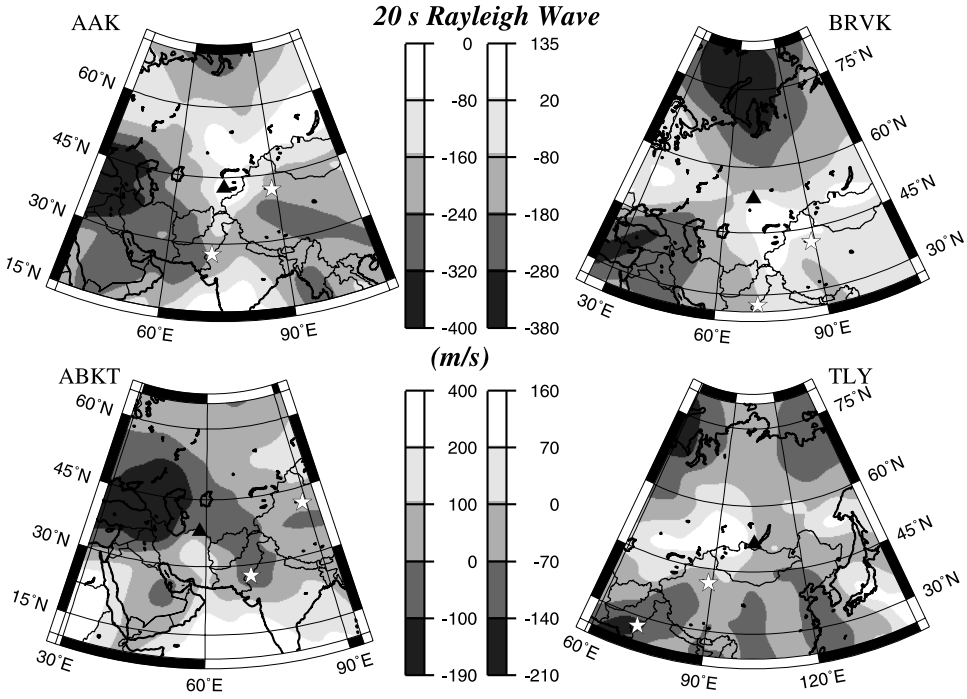

Figure 1
Group velocity correction surfaces for four stations in Central and Southern Asia for the 20 s Rayleigh wave. For each geographical point, the maps define the group velocity perturbation that should be applied to a 20 s Rayleigh wave observed at a station if an event were located at the chosen point. Perturbations are relative to the group velocity at the station. Units are m/s. The locations of the Chinese and Indian test sites are indicated with stars.

Kirghizstan), ABKT (Alibek, Turkmenistan), BRVK (Borovoye, Kazakhstan), and TLY (Talaya, Russia). For a given period, the value at each point on these maps represents the group velocity perturbation that a surface wave that originated at the point would experience if recorded on the specified station. The perturbations are relative to the group velocity at the station. In this form, group velocity maps can be used efficiently to predict dispersion curves for any event:station pair. BARMIN *et al.* (2001) present examples of group velocity correction surfaces for Rayleigh waves at 40 s period. We note two circumstances regarding the correction surfaces in Figure 1 and those shown by BARMIN *et al.* (2001). First, the corrections can be very large. For example, the 20 s Rayleigh wave from an event in the Caucasus 2500 km to AAK would experience a total group velocity perturbation of almost 400 m/s relative to the group velocity at AAK or a perturbation in arrival time of more than 2.5 minutes. Second, the correction surfaces at 20 s and 40 s are very different. This is because sedimentary basins control the 20 s map and crustal thickness controls the 40 s map.

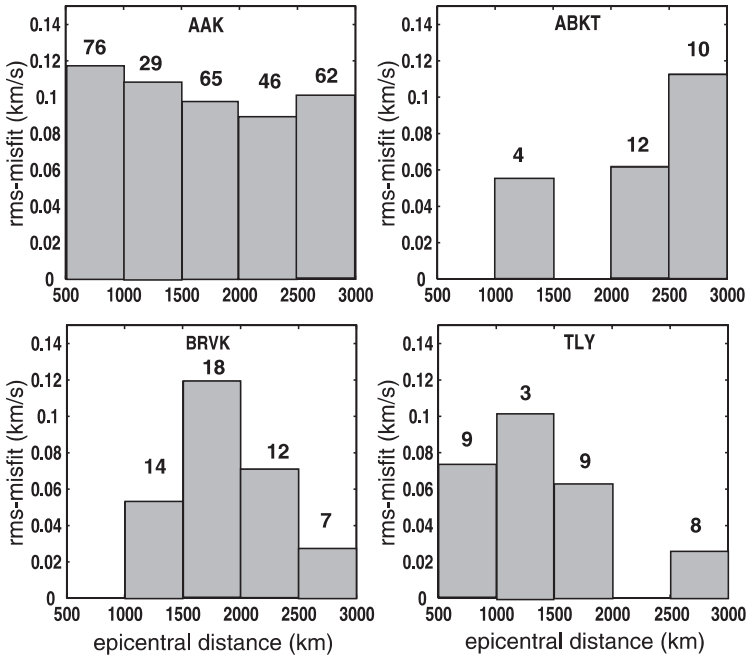

Figure 2
RMS-misfit between observed and predicted group velocities at four stations, plotted as a function of epicentral distance. Predicted group velocities are from RITZWOLLER *et al.* (1998). The measurements are from a database that includes earthquakes throughout Central and Southern Asia. The number of measurements per epicentral distance bin (summed over periods of 15 s, 20 s, and 25 s) is indicated above each histogram bar.

Figures 2–4 provide information about how well the correction surfaces constructed from the group velocity maps of RITZWOLLER *et al.* (1998) predict group velocity observations. Figure 2 shows the overall rms-misfit for the Rayleigh waves from 15 s–25 s period segregated by epicentral distance for observations made at four different stations. There is some indication of a diminishment of misfit with epicentral distance, and misfit is highly variable between stations. Misfit also varies strongly as a function of wave path. More or less homogeneous paths are fit better than paths through complicated structures. Figures 3 and 4 exemplify this. Figure 3 presents the observed group velocities between about 8 s and 35 s period obtained for the set of explosions and earthquakes on or near the Chinese Lop Nor test site, identified in Table 1. Because of the strong structural variability in Central Asia, there are very different dispersion curves observed at the different stations. The trends of the observed dispersion curves agree fairly well with those predicted from our group velocity maps. In the case of ABKT, however, the agreement is very poor, presumably because the path from Lop Nor to Turkmenistan is along structural gradients which complicate the wavefield in ways not represented by our group

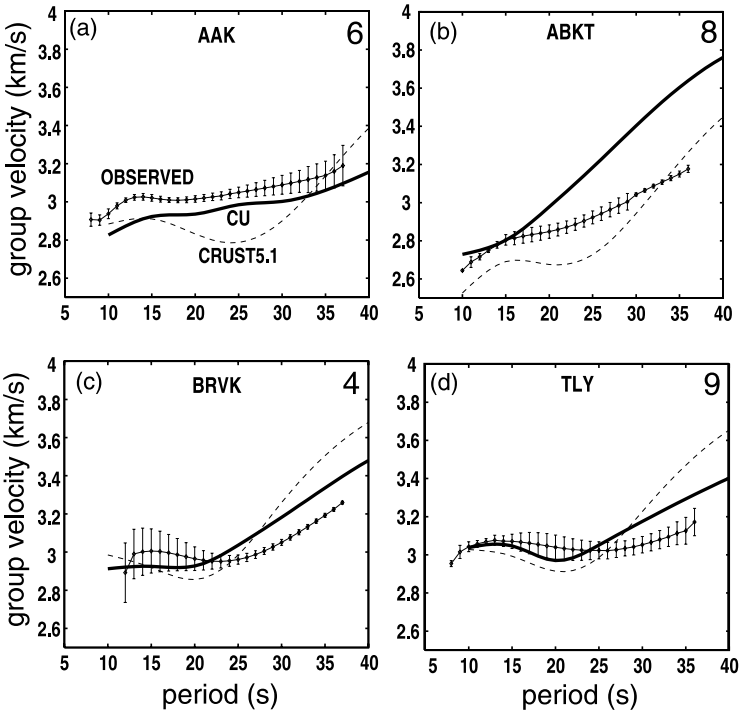

Figure 3

Comparison between observed and predicted group velocity curves. Group velocity measurements (error bars) at four stations in Central and Southern Asia following several nuclear explosions and earthquakes (Table 1) that occurred on or near the Lop Nor test site. The error bars represent the standard deviations of the measurements obtained at a given station following several Lop Nor events. The number of events used for each station is listed in the upper right-hand corner of each panel. Comparison is made with predictions RITZWOLLER *et al.* (1998) (solid line) and predictions from the hybrid crustal and mantle model CRUST5.1/S16B30 (dashed line).

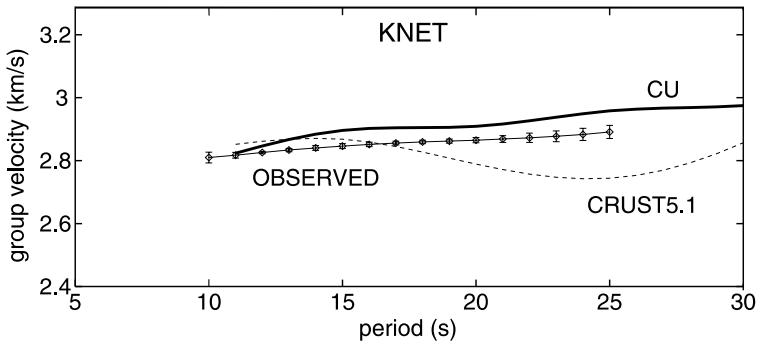

Figure 4

Like Figure 3, but for one of the Indian nuclear tests on May 11, 1998 observed at 5 stations of KNET.

Table 1

Events on or near the Lop Nor test site used in Figure 3

Event type	Date (mm/dd/yyyy)	Time (Z)	m_b	M_s
explosion	5/21/1992	4:59:57.5	6.5	5.0
explosion	10/5/1993	1:59:56.6	5.9	4.7
explosion	6/10/1994	6:25:57.8	5.8	–
explosion	10/7/1994	3:25:58.1	6.0	–
explosion	5/15/1995	4:05:57.8	6.1	5.0
explosion	8/17/1995	0:59:57.7	6.0	–
explosion	6/8/1996	2:55:57.9	5.9	4.3
explosion	7/29/1996	1:48:57.8	4.9	–
earthquake	9/25/1992	7:59:59.9	5.0	–
earthquake	11/27/1992	16:09:09.1	5.3	4.8
earthquake	12/26/1994	16:58:46.1	4.6	–
earthquake	3/18/1995	18:02:36.6	5.2	–
earthquake	3/20/1996	2:11:21.9	4.8	

velocity maps (e.g., LEVSHIN and RITZWOLLER, 1995). Another comparison is presented in Figure 4 however in this case we have clustered the measurements made at five stations in KNET to estimate the error bars. Agreement is fairly good in this case. On average, rms-misfit is less than about 100 m/s near 20 s period, which corresponds to an error in the predicted group travel time of less than 3%. The rms-misfit for the hybrid crustal and mantle model CRUST5.1/S16B30 (MASTERS *et al.*, 1996; MOONEY *et al.*, 1998) is about twice this value.

3. Phase Matched Filter for Automated Detection, Extraction, and Measurement

We describe here the method for detecting, extracting, and measuring surface waves. The method is entirely automated. We will describe the extraction and measurement first, assuming that the detection has been made and then will discuss the detector. To extract surface wave signals we use a phase-matched filter based on our group velocity correction surfaces, and to detect weak signals we simply allow the filter to slide along the time axis. The method of extraction and measurement is similar to that described by LEVSHIN *et al.* (1992), although here it has been automated.

Assume that the coordinates of the epicenter and the epicentral distance Δ to the station are approximately known. Let the surface wave signal $s(t)$ be

$$s(t) = \pi^{-1} Re \int_{\omega_0}^{\omega_1} |S(\omega)| e^{i(\omega t - \Psi(\omega))} \, d\omega \ , \tag{1}$$

where the origin time is assumed to be at zero time, $\Psi(\omega) = k(\omega)\Delta = \omega\Delta/C(\omega)$ is the negative of the phase spectrum relative to the origin time, $C(\omega)$ is the phase velocity

curve, k is wavenumber, and $|S(\omega)|$ is the amplitude spectrum of $s(t)$. The effects of dispersion on $s(t)$ are contained within the phase spectrum.

We wish to compress the signal by undispersing it in order to maximize the signal-to-noise ratio. To do this we would like to apply the correction $\psi(\omega) = \Psi(\omega)$, but typically we do not know the phase velocity or wavenumber curves reliably at periods below about 40 s. Thus we must estimate the phase correction either from a 3-D model or from group velocity maps. The 3-D model approach is taken by STEVENS and MCLAUGHLIN (2001) in this volume. The advantage of this approach is discussed further below. Models, however, are not as well resolved as group velocity maps and the signal-to-noise enhancement of the matched filter will depend on the accuracy and resolution of the dispersion maps used to undisperse the surface waves. In order to optimize resolution, we use recent group velocity maps to build the matched filter. To do so, we must utilize the relation between group and phase velocities, $U = d\omega/dk, C = \omega/k$, from which we see that:

$$k(\omega) = k_0 + \int_{\omega_0}^{\omega} \frac{d\omega'}{U(\omega')} \quad , \tag{2}$$

where

$$k_0 = \int_0^{\omega_0} \frac{d\omega'}{U(\omega')} \quad . \tag{3}$$

$U(\omega)$ is the group velocity curve, and the phase correction is

$$\psi(\omega) = k(\omega)\Delta \quad . \tag{4}$$

In practice, the continuous curve $U(\omega)$ is obtained by spline interpolating the discrete curve $U(T_i)$ from the group velocity maps for frequencies $\omega \in (\omega_0, \omega_1)$, the low and high cut-off frequencies of a bandpass filter applied to the observed seismogram. We typically construct the discrete curve $U(T_i)$ for each source-receiver pair from at a set of periods $T_i = 10, 15, 20, 25, 30, 35, 40$ s, set $2\pi/\omega_0 = 10$ s and $2\pi/\omega_1 = 40$ s, and taper quickly at the lower and higher frequencies. Using equations (2) and (4) we compute the envelope function $E(t)$ of the compressed or undispersed signal as follows:

$$E(t) = \pi^{-1} \left| \int_{\omega_0}^{\omega_1} |S(\omega)| \exp[i\omega t - i\Psi(\omega) + i\psi(\omega)]\, d\omega \right| \quad . \tag{5}$$

If the source time is known we apply the phase correction given by equation (5) described above to the spectrum of the observed seismogram and return to the time domain. If the group velocity curve is accurate this should have effectively undispersed the surface wave. We demonstrate this with applications to synthetic and real seismograms. Synthetics are computed by fundamental mode summation (e.g., LEVSHIN *et al.*, 1989) using a spherically symmetric model EUS. The velocities and Q values that define EUS are chosen to simulate stable, Eurasian structures. Compressed signals produced from the synthetic seismograms in Figure 5a are shown

in Figure 5b and from the real data following a large magnitude event shown in Figure 6a are contained in Figure 6b. Perfect compression would result in a sharply peaked function, as shown in the synthetic example. The example on real data is peaked, but not as sharply as the synthetic. Figure 5b shows that as the wave disperses, the amplitude of the compressed signal increases relative to the dispersed waveform. Thus, the signal-to-noise enhancement of the compressed signal grows with distance. The signal-to-noise enhancement at 1000 km in the synthetic example is about 20–30%, which is consistent with the ~20% enhancement observed on real data at 1200 km in Figure 6b.

To filter noise and unwanted signals we extract the compressed signal using a temporal window of fixed width centered on the peak of the compressed signal. The choice of the window width is *ad hoc*, however important. It should be broad enough to encompass the broadening of the compressed signal caused by the difference between the predicted and real dispersion curves, but narrow enough to filter out unwanted signals. Figure 2 demonstrates that for several stations in Central Asia using our entire surface wave database, the rms-misfit is less than about 100 m/s and is roughly independent of range below 3000 km. We find that a time window centered at the peak of the compressed signal with a full width in time corresponding to a group velocity range of about 200 m/s is broad enough to work in most cases. More work is still required to calibrate this width, perhaps increasing it in structurally complex regions and decreasing it elsewhere. Finally, we redisperse the extracted waveform by applying the inverse of the matched filter. Spectral amplitude as well as group and phase velocity are measured on the extracted waveform exactly as described by LEVSHIN *et al.* (1992) and RITZWOLLER and LEVSHIN (1998). In these papers, however, applications involved human interaction to control the waveform

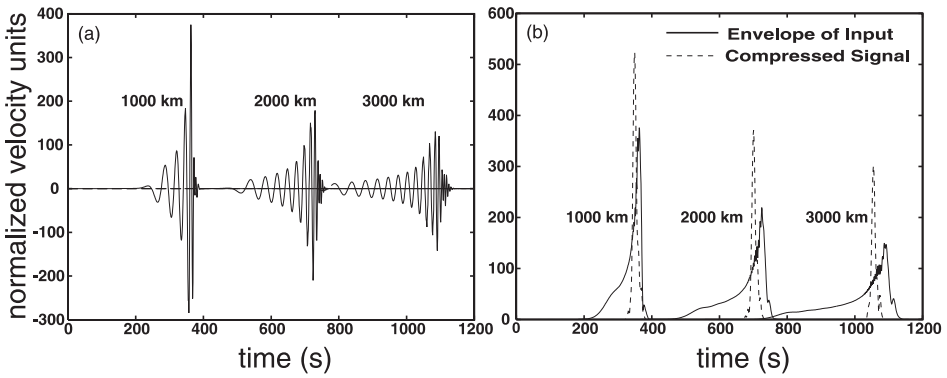

Figure 5
(a) Three synthetic Rayleigh waves computed for an explosive source at epicentral distances of 1000 km, 2000 km, and 3000 km. (b) The envelopes of the synthetic seismograms (solid lines) are compared with the envelopes of the compressed signals (dashed lines), $E(t)$, that result from the application of the phase-matched filter.

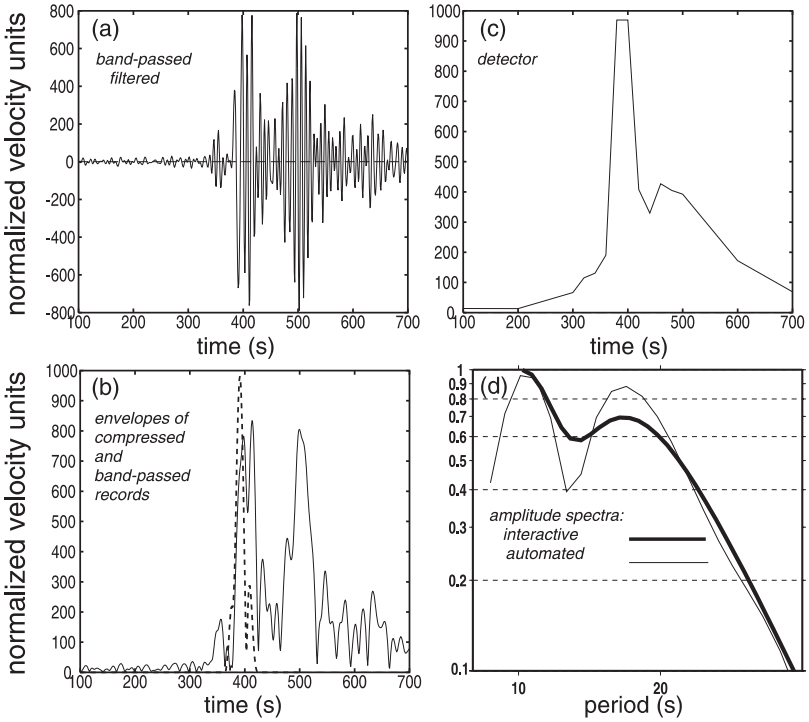

Figure 6

Demonstration of waveform compression, detection, and spectral amplitude estimation of strong surface wave signals. Nuclear explosion at the Lop Nor test site on June 8, 1996, $m_b = 5.9$, $\Delta \sim 1200$ km to AAK. (a) Band-passed (10 s^{-1}–40 s) vertical seismogram. The strong coda results from surface wave channeling by the Tarim Basin (LEVSHIN and RITZWOLLER, 1995). (b) Comparison of the envelopes of the band-passed filtered seismogram (solid line) and the compressed signal (dashed line). The compressed signal, $E(t)$, results from the application of the phase-matched filter. (c) Peak amplitude of the envelope of the compressed signal, $D(t - t_0)$, plotted for origin times from several minutes before to several minutes after the PDE origin time. (d) Rayleigh wave spectrum found by automated frequency-time analysis compared with the spectrum obtained with human interaction during the frequency-time analysis.

extraction. This method is adaptive in that it finds the dispersion ridge and measures amplitudes and velocities on the ridge. Figure 6d presents an example of an automated spectral amplitude compared with the spectral amplitude estimated with human interaction to define the extraction filter. Discrepancies of 20% may exist below 20 s period, particularly near spectral holes.

In the description above we have glossed over an important subtlety. Knowledge of the phase correction, $\psi(\omega)$, requires us to know k_0, which in turn depends on an estimate of $U(\omega)$ to zero frequency. In fact, we estimate $U(\omega)$ only above some minimum frequency, ω_0. The result is that we only know $\psi(\omega)$ reaching a constant of unknown value equal to $k_0\Delta$. Thus the resulting envelope function will appear shifted in time by about $k_0\Delta$ from where it would appear if we knew the phase correction

perfectly. The shift will always be toward shorter times relative to the location with the unknown constant included. Notice in Figure 5b that the location of the compressed signal marches to earlier times relative to the peak of the envelope of the uncompressed signal as the epicentral distance is increased. This uncertainty in the location of the envelope of the compressed signal is no obstacle for most purposes, because we make no measurements on the compressed signal. Rather in our applications the compressed signal exists only to improve the detectability and to facilitate the extraction of the surface waves. All measurements are made when the signals have been uncompressed or redispersed. In the process of uncompression the time uncertainty that is introduced by compression is reversed and the extracted waveform suffers no distortions in time. However, if the compressed signal would have resulted from a highly accurate phase correction, then the peak times of the compressed signal could be used to locate the event. Event location with weak surface wave signals probably is not a major desirable at this time. If it becomes important in the future and if 3-D models improve substantially in order to ensure the accuracy of the predicted phase velocity curves, then the model based method of STEVENS and MCLAUGHLIN (2001) would be preferable to the method we discuss here.

If the source time is not known, the method we describe above may be naturally used to detect weak surface wave signals. We simply vary the source time, t_0, in a systematic way and plot the peak amplitude of the envelope of the compressed signal for each source time. We call this the detector time series, $D(t - t_0)$, which is a time series of amplitudes that will peak near the travel time of the compressed signal from the source. Signals with phase-content similar to the phase-matched filter are amplified and other signals are reduced. Figure 6c shows an example of a strong event. The signal-to-noise ratio (SNR) of this detection is about 75:1. Therefore, the detector clearly has identified a signal. Strong detections need not be delta-like. The detector time series in Figure 6c displays a hump following the main detection caused by surface wave energy scattered into the Tarim Basin (LEVSHIN and RITZWOLLER, 1995). Figure 7 demonstrates that the detector based on our group velocity maps works considerably better than one based on the spherically symmetric model EUS. The signal-to-noise ratio of the detector time series is usually about 1.5 times higher using the group velocity maps than the model EUS.

4. Preliminary Application to Weak Events

The detection of strong events, such as the example in Figure 6, is straightforward. Detection and spectral estimation of weak events is the motivation of this study, however. We have applied the detector/extractor/spectral estimator to broadband records following a number of weak events at the Lop Nor, China test site and one of the nuclear explosions at the Indian Rajasthan test site that occurred on May 11, 1998.

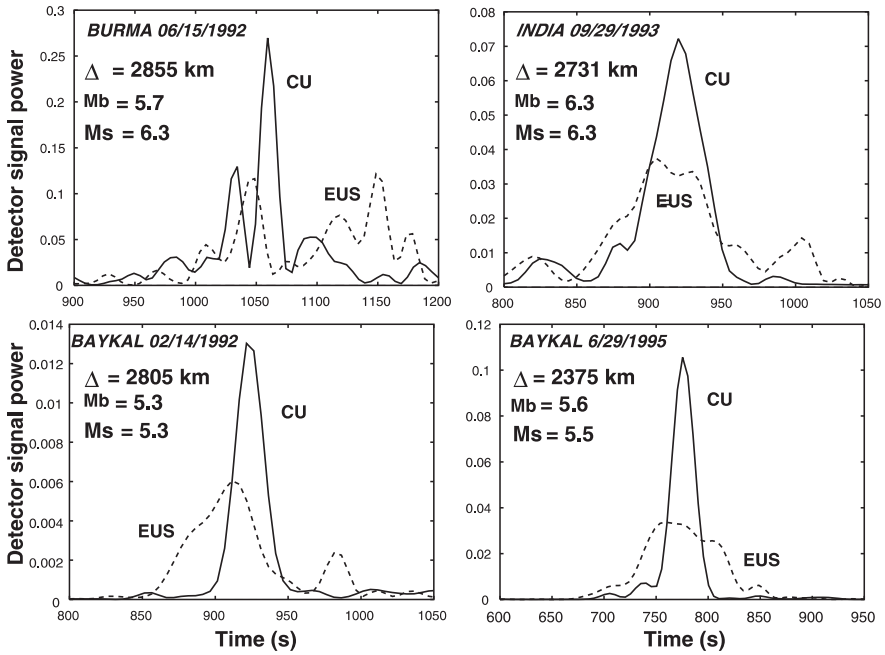

Figure 7
Comparison of the effectiveness of the automated detector based on two different group velocity correction surfaces: the group velocity maps of RITZWOLLER *et al.* (1998) denoted as CU (solid lines) and the group velocity curve predicted by an average model of the crust and uppermost mantle for Eurasia denoted as EUS (dashed lines). All measurements are from the station AAK and the event location is indicated in each panel. Signal compression and hence detection is greatly improved with the group velocity maps.

Figure 8 shows the results for a nuclear test at Lop Nor with $m_b = 4.9$ that occurred on July 29, 1996. The M_s of this event is probably in the middle to high 3's, because, as Table 1 shows, the M_s for nuclear explosions at Lop Nor is usually more than a magnitude unit below m_b. As can be seen in Figure 8, the surface wave can barely be discerned on raw or band-passed records. However, the detection algorithm described above demonstrates a clear detection with a SNR of about 4:1, and the automated amplitude estimate approximates that which is obtained with direct human interaction.

Figure 9 presents similar results for the Indian test. However, for the Indian test we have applied the method to five stations of KNET. The stations are located in structurally very different areas, and this apparently manifests itself as substantial differences in the observed amplitude spectra below about 18 s period. These differences are borne out when the measurements are obtained with human interaction. This highlights the difficulty in reducing the period at which M_s is measured below its current value of 20 s. Near-receiver structural variations with spatial scales well below the resolution of group velocity maps or 3-D models can result in amplitude effects as large as 50% at periods below 15 s.

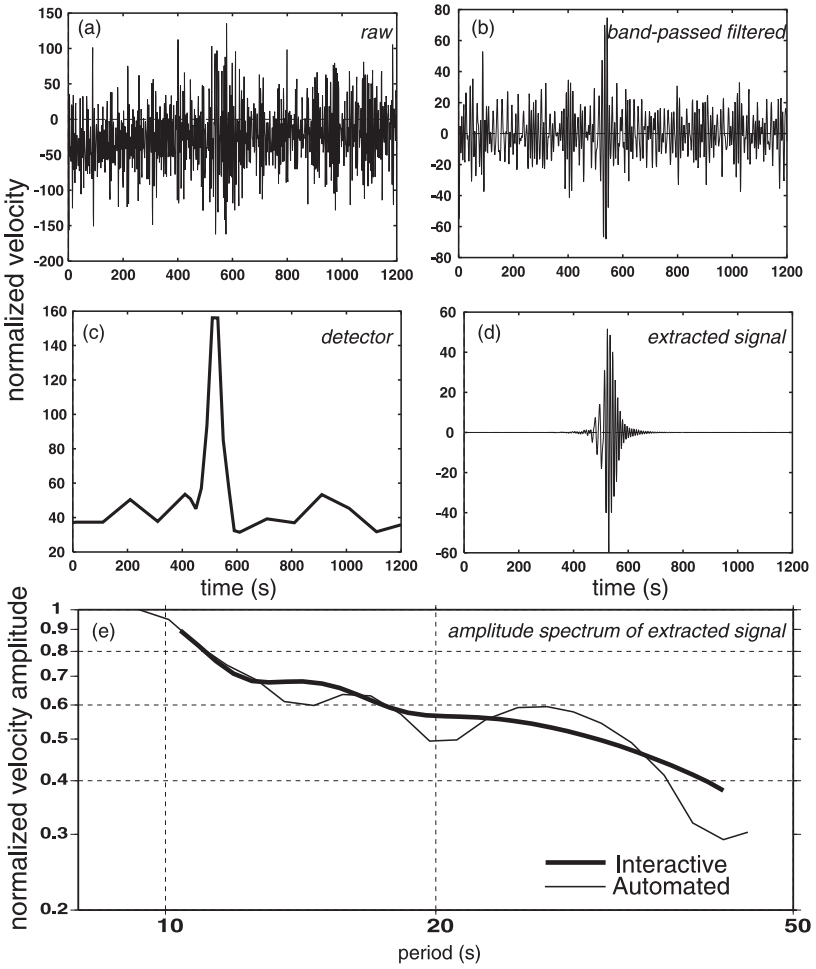

Figure 8

Demonstration of the detection, extraction, and spectral amplitude estimation of weak surface wave signals. Nuclear explosion at the Lop Nor test site on July 29, 1996, $m_b = 4.9$, $\Delta \sim 1600$ km to TLY. (a) Raw vertical seismogram observed at TLY following a nuclear explosion at Lop Nor. (b) Band-passed (10 s–40 s) seismogram. (c) Same as Figure 6c. (d) Extracted waveform on which the spectral amplitude measurement is obtained. (e) Rayleigh wave spectrum found by the automated frequency-time analysis compared with the spectrum obtained with human interaction during the frequency-time analysis.

5. Conclusions

We describe an automated surface wave detector and extractor designed to work on weak surface wave signals across Eurasia at intermediate periods (8 s–40 s). The method is based on phase-matched filters defined by the Rayleigh wave group travel-time predictions from the broadband group velocity maps presented by RITZWOLLER

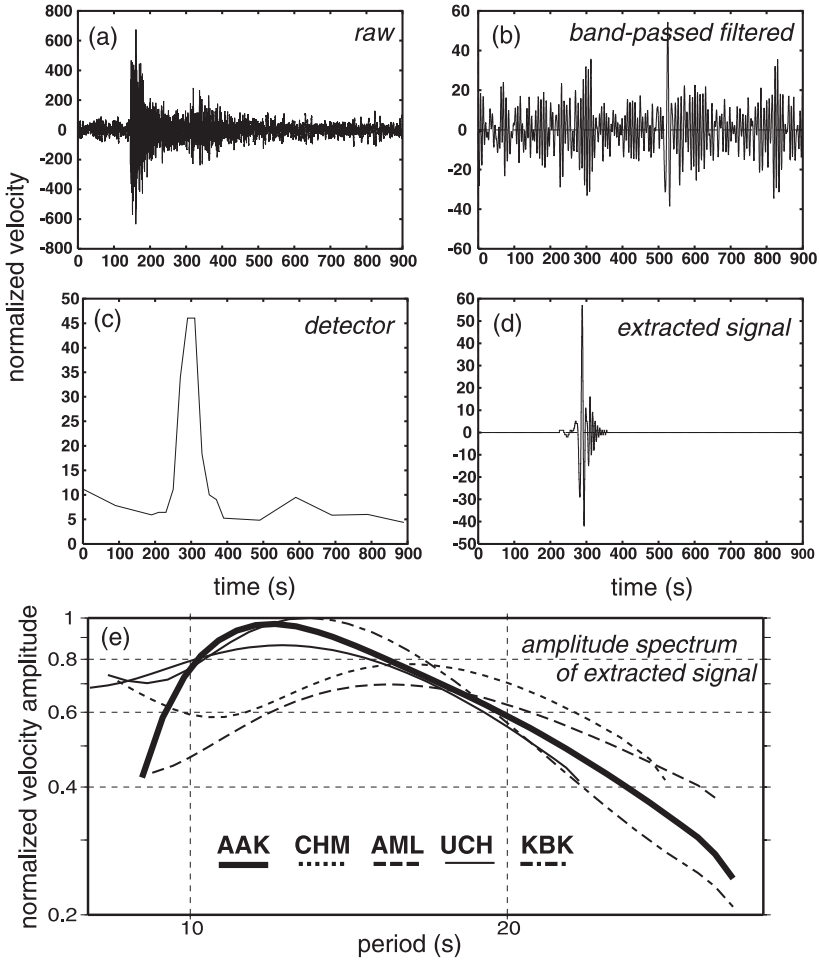

Figure 9
Same as Figure 8, but for a nuclear test in India. Nuclear explosion at the Rajasthan test site on May 11, 1998, $m_b = 5.1$, $\Delta \sim 1700$ km to KNET. The spectral amplitude measurements are at five KNET stations. Panels (a)–(d) are for AAK.

and LEVSHIN (1998) and RITZWOLLER *et al.* (1998). We describe preliminary results of the application of this method to a set of nuclear explosions and earthquakes in Central Asia. These and other applications lead us to conclude that this method shows considerable promise as a surface wave detector and of yielding high quality surface wave measurements automatically. It appears to be feasible to obtain automated spectral amplitude measurements for events in Central and Southern Asia with M_s down to as low as 3.5–4.0.

The method, however, requires further tuning and a more complete statistical evaluation. As discussed above, the extraction algorithm requires further work in

that we need to calibrate the width of the temporal extraction window. The quality of the automated measurements and the SNR of the detection depend on the accuracy of the group velocity maps from which the phase-matched filter is defined. For example, more accurate maps allow sharper temporal filters to be applied which reduces bias in amplitude and velocity measurements caused by coda, multipathing, etc. The group velocity maps will continue to be improved and we anticipate improved performance when they are used. A more complete statistical evaluation of the automated spectral amplitude and velocity measurements relative to measurements obtained with human interaction would also be valuable. Finally, a more complete statistical evaluation of the detector is in order. In particular, the frequency and character of false-alarms and missed events should be characterized and a more complete comparison of the signal-to-noise characteristics of the detector based on our dispersion maps and earlier models should be performed.

Acknowledgments

We would like to thank Antonio Villaseñor for his valuable review and the staff at the IRIS DMC for providing the broad digital data used in this research. All maps were generated with the Generic Mapping Tools (GMT) data processing and display package (Wessel and Smith, 1991, 1995). This work was supported by DSWA contract 001-97-C-0157.

References

Barmin, M. P., Ritzwoller, M. H., and Levshin, A. L. (2001), *A Fast and Reliable Method for Surface Wave tomography*, Pure appl. geophys., this volume.

Cara, M. (1973), *Filtering of Dispersed Wavetrains*, Geophys. J. R. astr. Soc. *33*, 65–80.

Dziewonski, A., Bloch, S., and Landisman, N. (1969), *A Technique for the Analysis of Transient Seismic Signals*, Bull. Seismol. Soc. Am. *59*, 427–444.

Herrin, E., and Goforth, T. (1977), *Phase-matched Filters: Application to the Study of Rayleigh Waves*, Bull. Seismol. Soc. Am. *67*, 1259–1275.

Levshin, A. L., and Ritzwoller, M. H. (1995), *Characteristics of Surface Waves Generated by Events on and near the Chinese Nuclear Test Site*, Geophys. J. Int. *123*, 131–149.

Levshin, A. L., Pisarenko, V. F., and Pogrebinsky, G. A. (1972), *On a Frequency-time Analysis of Oscillations*, Ann. Geophys. *28*, 211–218.

Levshin, A. L., Ratnikova, L., and Berger, J. (1992), *Peculiarities of Surface Wave Propagation across Central Eurasia*, Bull. Seismol. Soc. Am. *82*, 2464–2493.

Levshin, A. L., Yanovskaya, T. B., Lander, A. V., Bukchin, B. G., Barmin, M. P., Ratnikova, L. I., and Its, E. N. *Seismic Surface Waves in a Laterally Inhomogeneous Earth* (V. I. Keilis-Borok, ed.) (Kluwer Publ., Dordrecht, 1989).

Levshin, A. L., Ritzwoller, M. H., Barmin, M. P., Villaseñor, A., and Padgett, C. A. (2001), *New Constraints on the Arctic Crust and Uppermost Mantle: Surface Wave Group Velocities, P_n, and S_n*, Phys. Earth Planet. Int. *123*, 185–204.

Masters, G., Johnson, S., Laske, G., and Bolton, H. (1996), *A Shear-velocity Model of the Mantle*, Phil. Trans. R. Soc. Lond. *A 354*, 1385–1411.

MOONEY, W. D., LASKE, G., and MASTERS, G. (1998), *CRUST 5.1: A Global Crustal Model at 5 Degrees by 5 Degrees*, J. Geophys. Res. *103*, 727–748.

REZAPOUR, M., and PEARCE, R. G. (1998), *Bias in Surface Wave Magnitude M_s due to Inadequate Distance Corrections*, Bull. Seismol. Soc. Am. *88*, 43–61.

RITZWOLLER, M. H., and LEVSHIN, A. L. (1998), *Eurasian Surface Wave Tomography: Group Velocities*, J. Geophys. Res. *103*, 4839–4878.

RITZWOLLER, M. H., LEVSHIN, A. L., RATNIKOVA, L. I., and EGORKIN, A. A. (1998), *Intermediate Period Group Velocity Maps across Central Asia, Western China, and Parts of the Middle East*, Geophys. J. Int. *134*, 315–328.

RUSSELL, D. W., HERRMANN, R. B., and HWANG, H. (1988), *Application of Frequency-variable Filters to Surface Wave Amplitude Analysis*, Bull. Seismol. Soc. Am. *78*, 339–354.

STEVENS, J. L. (1986), *Estimation of Scalar Moments from Explosion-generated Surface Waves*, Bull. Seismol. Soc. Am. *76*, 123–151.

STEVENS, J. L., and MCLAUGHLIN, K. L. (1997), *Improved methods for regionalized surface wave analysis*. In Proceed. 19th Seismic Res. Symp. on Monitoring a CTBT, pp. 171–180.

STEVENS, J. L., and MCLAUGHLIN, K. L. (2001), *Optimization of Surface Wave Identification and Measurement*, this volume.

VDOVIN, O. Y. (1999), *Surface Wave Tomography of South America and Antarctica*, Ph.D. Thesis, Department of Physics, University of Colorado at Boulder.

VDOVIN, O. Y., RIAL, J. A., LEVSHIN, A. L., and RITZWOLLER, M. H. (1999), *Group Velocity Tomography of South America and the Surrounding Oceans*, J. Geophys. Res. *136*, 324–330.

WESSEL, P., and SMITH, W. H. F. (1991), *Free Software Helps Map and Display Data*, EOS Trans. AGU *72*, 441.

WESSEL, P., and SMITH, W. H. F. (1995), *New Version of the Generic Mapping Tools Released*, EOS Trans. AGU *76*, 329.

(Received February 20, 2000, revised May 25, 2000, accepted June 15, 2000)